carotid sinus pressure (CSP), sympathetic nerve activity (SNA) and systemic arterial pressure (AP) during CSP perturbation in open-loop baroreflex condition. CSP is changed according to a binary random (white-noise) signal with a switching interval of 500 ms. **B**: Input power spectrum of CSP (green line) is reasonably flat up to 1 Hz. Autospectra of SNA (top line) and systemic AP (bottom line) are also shown. The arrowhead indicates a peak of SNA autospectrum at 0.4 Hz. **C**: Open-loop transfer functions of the neural arc ($H_{n\text{-}open}$) from CSP input to SNA (left panels) and of the peripheral arc ($H_{p\text{-}open}$) from SNA input to AP (right panels) identified in the same animal as in A. The gain (top), phase (second), coherence (third) and normalized random error (Error, bottom) functions are shown. **D**: Step responses (Step res.) derived from the transfer functions shown in **C**. **E**: Open-loop transfer functions of the total arc ($H_{total\text{-}open}$) from CSP input to AP identified in the same animal as in A. The gain (top), phase (second), coherence (third) and normalized random error (Error, bottom) functions are shown. **F**: Step response (Step res.) derived from the transfer function shown in **E**. a.u., arbitrary unit.

Figure 4. **A**: Typical representative data of protocol 3, showing time series of CSP, SNA and systemic AP in closed-loop-spontaneous baroreflex condition, where CSP is matched with systemic AP. The data were obtained from the same animal as in Figure 3. **B-D** show exactness of good match between CSP and systemic AP. **B**: Autospectrum of CSP (green line) overlaps with that of AP (black line). Autospectrum of SNA (top line) is also shown. The arrowhead indicates a peak in the SNA autospectrum at 0.4 Hz. **C**: Beat-to-beat waveform of CSP (green line) overlaps with that of AP (black line). **D**: The transfer functions from CSP to systemic AP. Gain (top), phase (middle) and coherence (bottom) functions are shown. **E**: The closed-loop-spontaneous transfer functions of the neural arc ($H_{n\text{-}closed\text{-}spon}$) from CSP (=AP) input to SNA (left panels) and of the peripheral arc ($H_{p\text{-}closed\text{-}spon}$) from SNA input to AP (right panels) identified in the same animal as in A. The gain (top), phase (second), coherence (third) and normalized random error (bottom) functions are shown. **F**: Step responses (Step res.) derived from the transfer functions. a.u., arbitrary unit; CSP, carotid

sinus pressure; SNA, sympathetic nerve activity; AP, arterial pressure; Step res., step response. In **E** and **F**, the open-loop transfer functions and derived step responses are included for reference (red lines).

Figure 5. Transfer functions obtained from all animals (n = 10). Solid and dashed lines represent the mean and mean + SD, respectively. **A**: Red lines are open-loop transfer functions of the neural ($H_{n\text{-}open}$, left panels) and peripheral arcs ($H_{p\text{-}open}$, right panels) identified in protocol 1. The gain (top), phase (second), coherence (third) and normalized random error (bottom) functions are shown. Blue lines are closed-loop-spontaneous transfer functions (blue lines) of the neural ($H_{n\text{-}closed\text{-}spon}$, left panels) and peripheral arcs ($H_{p\text{-}closed\text{-}spon}$, right panels) identified in protocol 2. The closed-loop-spontaneous baroreflex transfer function for the neural arc is markedly different from the open-loop transfer function, whereas that for the peripheral arc partially matches the open-loop transfer function. **B**: Step response calculated from the open-loop (red lines) and closed-loop-spontaneous (blue lines) transfer functions. a.u., arbitrary unit; CSP, carotid sinus pressure; SNA, sympathetic nerve activity; AP, arterial pressure; Step res., step response.

Figure 6. **A**: Typical representative example of evaluating the predictability of SNA output from CSP input using the baroreflex transfer functions of the neural arc. The data were obtained from the same animal as in Figure 3. The time-series SNA dynamics are predicted from CSP measured in protocol 4 (top panel), by the open-loop transfer function determined in protocol 1 (red line, third panel) and by the closed-loop-spontaneous transfer function determined in protocol 2 (blue line, bottom panel). CSP is changed according to a binary random (white-noise) signal with a switching interval of 500 ms under open-loop baroreflex condition. These predicted SNA changes are compared with the actual SNA measured in protocol 4 (second panel). SNA (red line, third panel) predicted by open-loop transfer function ($H_{n\text{-}open}$) appears to parallel the actually measured SNA, whereas SNA predicted by closed-loop-spontaneous transfer function ($H_{n\text{-}closed\text{-}spon}$) is markedly different from the

measured SNA. **B**: Scatter plot analysis of the SNA predicted by $H_{n\text{-}open}$ versus the measured SNA. **C**: Scatter plot analysis of the SNA predicted by $H_{n\text{-}closed\text{-}spon}$ versus the measured SNA.

Figure 7. **A**: Typical representative example of evaluating the predictability of AP output from SNA input using baroreflex transfer functions of the peripheral arc. The data were obtained from the same animal as in Figure 3. The time-series AP dynamics are predicted from SNA measured in protocol 4 (top panel), by the open-loop transfer function determined in protocol 1 (red line, third panel) and by the closed-loop-spontaneous transfer function determined in protocol 2 (blue line, bottom panel). These predicted AP changes are compared with the actual AP measured in protocol 4 (the gray and black lines indicate AP resampled at 10 and 1 Hz, respectively; second panel). AP predicted by open-loop transfer function ($H_{p\text{-}open}$) appears to parallel the actually measured AP, whereas AP predicted by closed-loop-spontaneous transfer function ($H_{n\text{-}closed\text{-}spon}$) also correlates to some extent. **B**: Scatter plot analysis of the AP predicted by $H_{p\text{-}open}$ versus the measured AP. **C**: Scatter plot analysis of the AP predicted by $H_{p\text{-}closed\text{-}spon}$ versus the measured AP.

Figure 8. **A:** Example of spontaneous changes in AP (resampled at 10 and 0.1 Hz represented by black and gray lines, respectively, in the top panel) and SNA (resampled at 10 and 0.1 Hz in second and third panels, respectively) in closed-loop baroreflex condition (protocol 5). Using the open-loop ($H_{n\text{-}open}$, identified in protocol 1) and the closed-loop-spontaneous transfer functions ($H_{n\text{-}closed\text{-}spon}$, identified in protocol 2) of the neural arc, a time-series of SNA output was predicted from the actual AP measured in protocol 5. However, the predicted SNA (resampled at 10 Hz represented by gray line, and at 0.1 Hz represented by red and blue lines in fourth and bottom panels, respectively) response is markedly different from the trend of measured SNA. **B**: Scatter plot analysis of the SNA predicted by $H_{n\text{-}open}$ versus the measured SNA. **C**: Scatter plot analysis of the SNA predicted by $H_{n\text{-}closed\text{-}spon}$ versus the measured SNA.

Figure 9. **A**: Example of spontaneous changes in SNA (resampled at 10 and 0.1 Hz in top and second panels, respectively) and AP (resampled at 10 and 0.1 Hz represented by gray and black lines, respectively, in third panel) under closed-loop baroreflex condition measured in protocol 5. Using the open-loop transfer function ($H_{p\text{-}open}$, identified in protocol 1) and the closed-loop-spontaneous transfer function ($H_{p\text{-}closed\text{-}spon}$, identified in protocol 2) of the peripheral arc, a time-series of AP output was predicted (resampled at 10 Hz represented by gray line, and at 0.1 Hz represented by red and blue lines in fourth and bottom panels, respectively) from the actual SNA measured in protocol 5. The predicted APs resampled at 0.1 Hz appear similar to the measured AP to some extent. **B**: Scatter plot analysis of the AP predicted by $H_{p\text{-}open}$ versus the measured AP. **C**: Scatter plot analysis of the AP predicted by $H_{p\text{-}closed\text{-}spon}$ versus the measured AP.

Figure 10. **A**: Example of changes in CSP and AP (resampled at 10 Hz in the top and second panels, respectively) induced by pharmacological interventions and SNA responses (resampled at 10 and 0.1 Hz represented by gray and black lines, respectively, in third panel) in closed-loop baroreflex condition (protocol 5). Sequential bolus infusions of phenylephrine (P_1), nitroprusside (N) and phenylephrine (P_2) were administered. Using the open-loop ($H_{n\text{-}open}$, identified in protocol 1) and the closed-loop-spontaneous transfer functions ($H_{n\text{-}closed\text{-}spon}$, identified in protocol 2) of the neural arc, time-series of SNA output was predicted (resampled at 10 Hz represented by gray line, and at 0.1 Hz represented by red and blue lines in fourth and bottom panels, respectively) from the actual AP measured in protocol 5. SNA predicted by open-loop transfer function ($H_{n\text{-}open}$) appears to parallel the actually measured SNA, whereas SNA predicted by closed-loop-spontaneous transfer function ($H_{n\text{-}closed\text{-}spon}$) is markedly different from the measured SNA. **B**: Scatter plot analysis of the SNA predicted by $H_{n\text{-}open}$ versus the measured SNA. The identity line is shown. **C**: Scatter plot analysis of the SNA predicted by $H_{n\text{-}closed\text{-}spon}$ versus the measured SNA. **D**: Relationship between CSP and SNA predicted by $H_{n\text{-}open}$ (red filled circle, red broken line) is

similar to that between CSP and actually measured SNA (open circle, black broken line) or **E**: Relationship between CSP and SNA predicted by $H_{n\text{-}closed\text{-}spon}$ (blue filled circle, blue broken line) is different from that between CSP and actually measured SNA (open circle, black broken line).

Figure 11. A numerical simulation of the effects of noise on calculation of baroreflex transfer functions. Noise (Gaussian white-noise) is introduced to the neural and/or peripheral arcs in closed-loop-spontaneous baroreflex condition, where CSP equals AP (see Figure 1C).

A: The original baroreflex transfer functions of the neural (H_n, left panel) and peripheral (H_p, right panel) arcs. H_n is modelled using derivative and high-cut filter characteristics with a pure delay, and $H_{p\text{-}open}$ using the second-order low-pass filter with a pure delay (see APPENDIX B).

B-D: Block diagrams (upper panels) and closed-loop-spontaneous transfer functions (lower panels); calculated from AP to SNA as the neural arc (left lower panel) and from SNA to AP as the peripheral arc (right lower panel). The open-loop transfer functions (H_n, H_p) are included as reference (gray lines). **B**: First simulation: noise (0.029, 0.117, 0.264, 0.732 and 2.928 x 10^3 au^2) is present only in the neural arc. The same results are obtained irrespective of the noise intensity. The closed-loop-spontaneous transfer function of the neural arc is totally different from the open-loop transfer function H_n, whereas that of the peripheral arc overlaps with H_p. **C**: Second simulation: noise (0.029, 0.117, 0.264, 0.732 and 2.928 x 10^3 $mmHg^2$ is present only in the peripheral arc. The same results are obtained irrespective of the noise intensity. The closed-loop-spontaneous transfer function of the neural arc overlaps the open-loop transfer function H_n, whereas that of the peripheral arc is markedly different from H_p. **D**: Third simulation: noise with incremental intensity [from 0.029 (broken line) to 0.117, 0.264, 0.732 and 2.928 (solid lines) x 10^3 au^2] is present in the neural arc, while a small constant noise (29 $mmHg^2$) is present in the peripheral arc. The closed-loop-spontaneous transfer function of the neural arc is different from the open-loop

transfer function of H_n, whereas that of the peripheral arc approaches H_p and the two become overlapped as the noise in the neural arc increases. H_n, neural arc transfer function; H_p, peripheral arc transfer function, NN, unknown neural noise; PN, unknown peripheral noise.

Figure 1

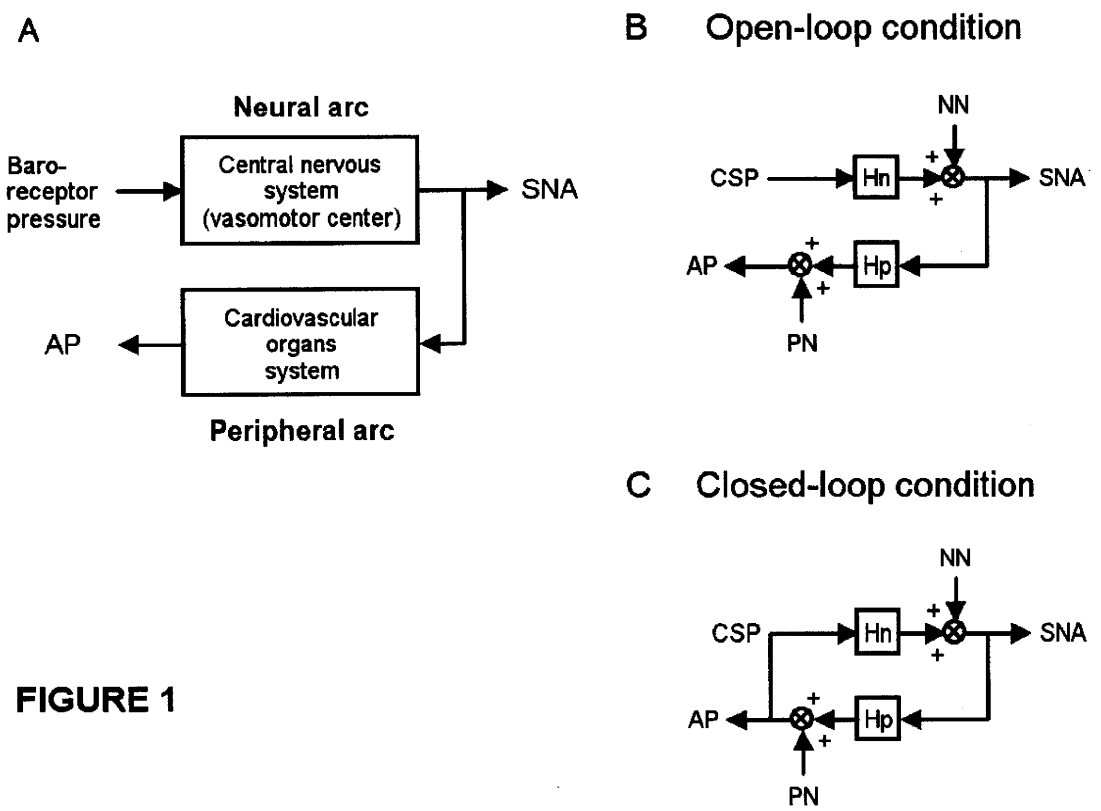

FIGURE 1

Figure 2

FIGURE 2

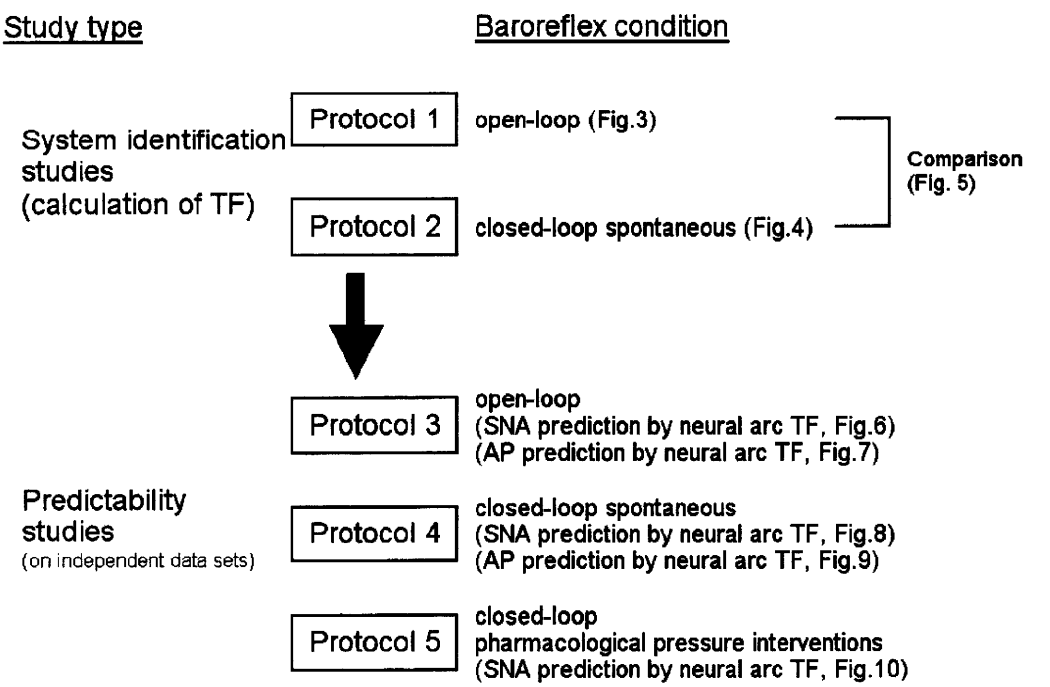

Figure 3

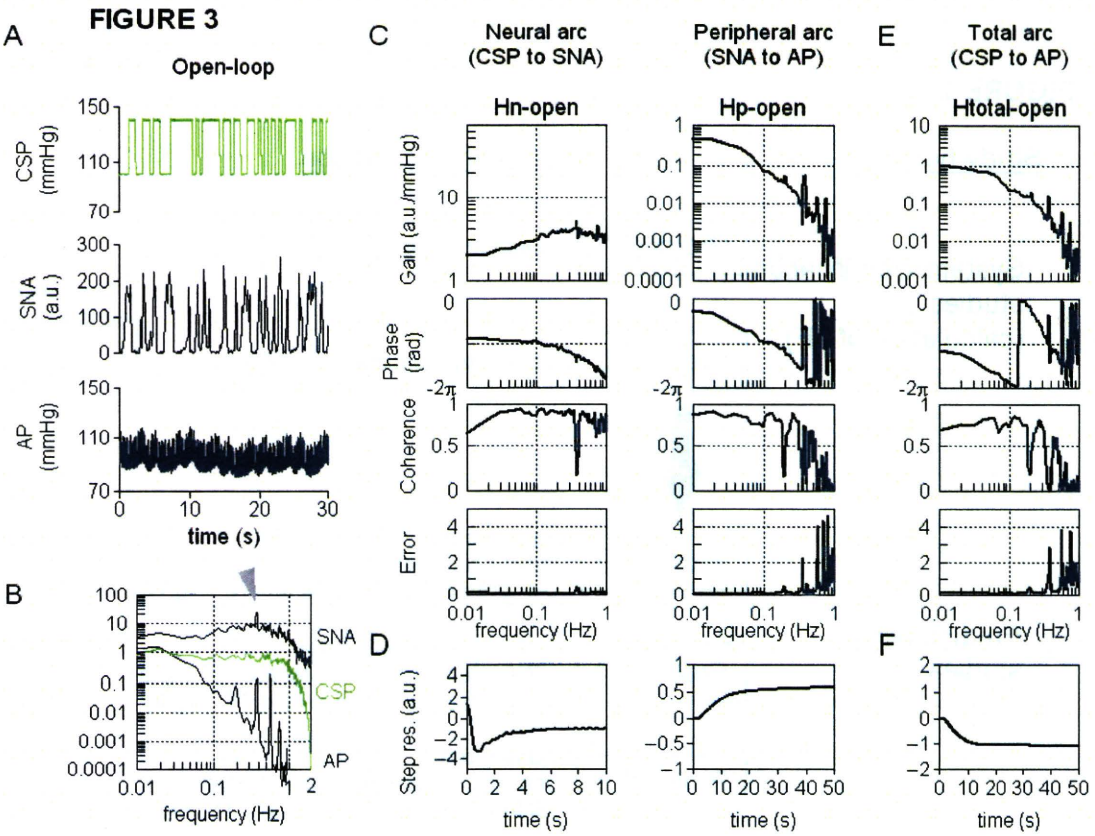
FIGURE 3
A
Open-loop
CSP (mmHg)
SNA (a.u.)
AP (mmHg)
time (s)
B
SNA
CSP
AP
frequency (Hz)
C
Neural arc (CSP to SNA)
Peripheral arc (SNA to AP)
E
Total arc (CSP to AP)
Hn-open
Hp-open
Htotal-open
Gain (a.u./mmHg)
Phase (rad)
Coherence
Error
frequency (Hz)
D
Step res. (a.u.)
time (s)
F
time (s)

Figure 4

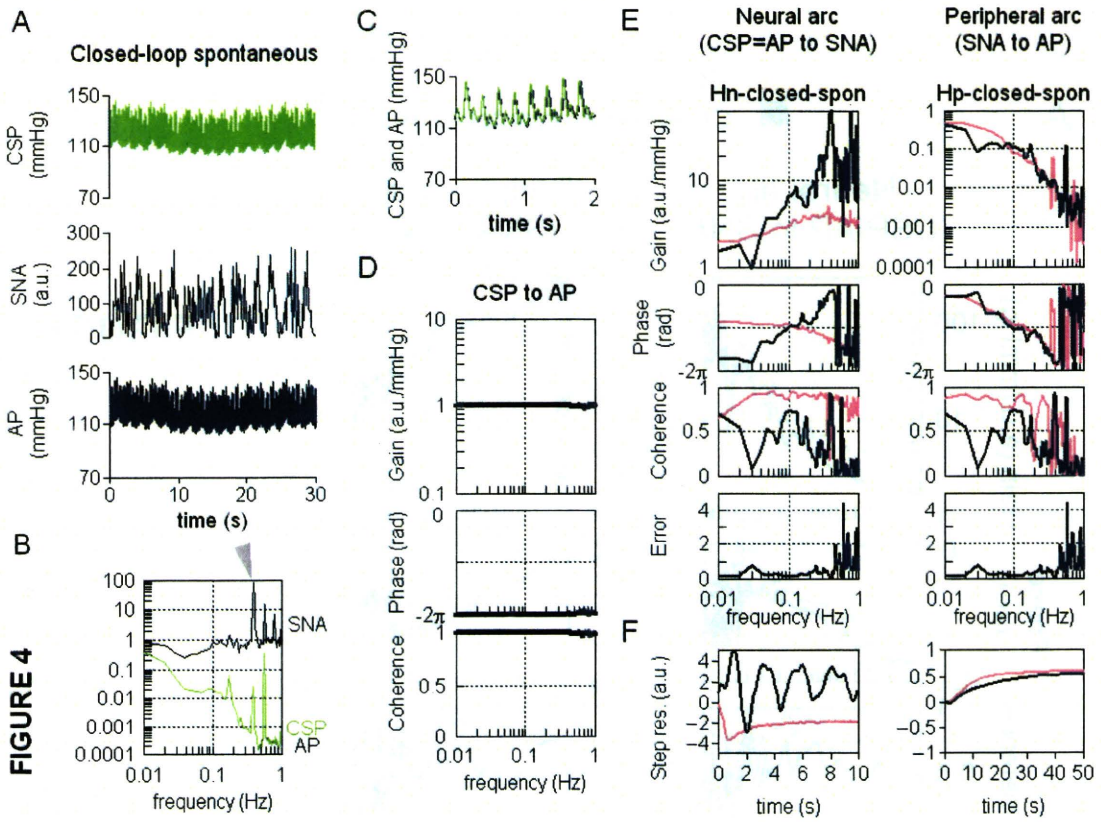

FIGURE 4

Figure 5

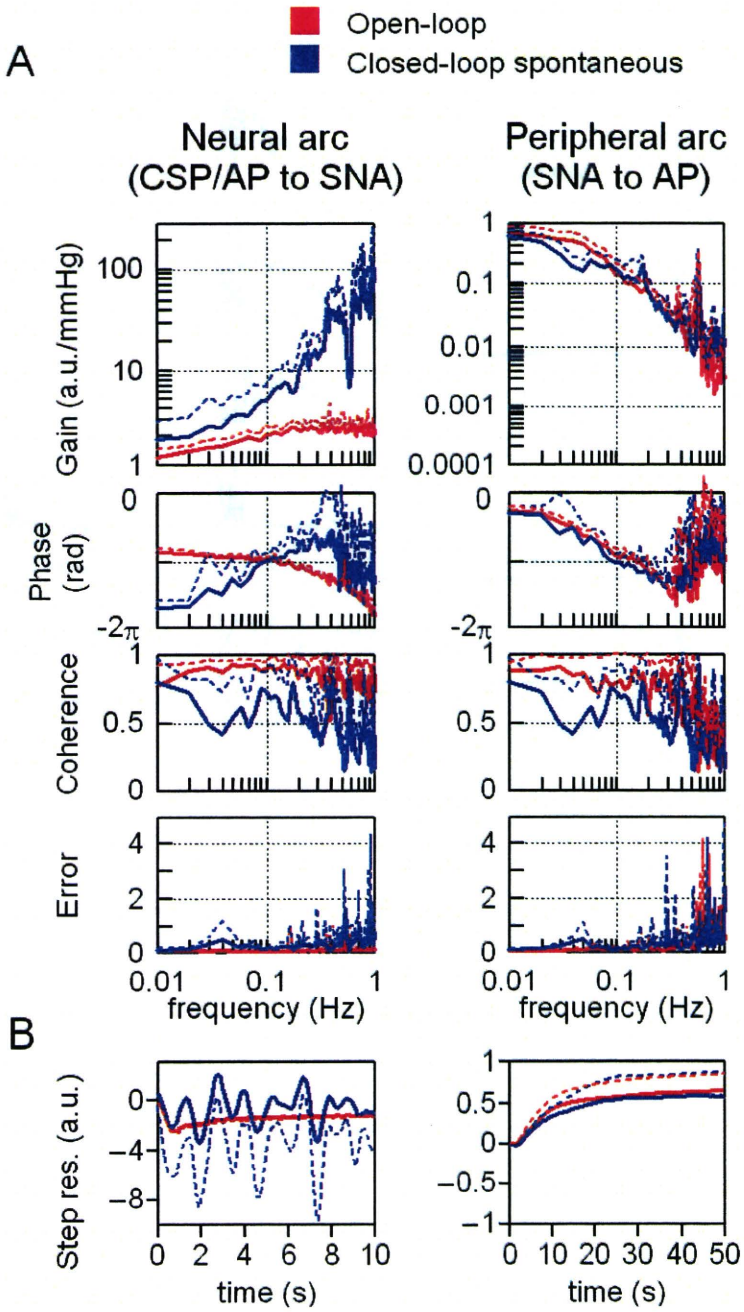

FIGURE 5

Figure 6

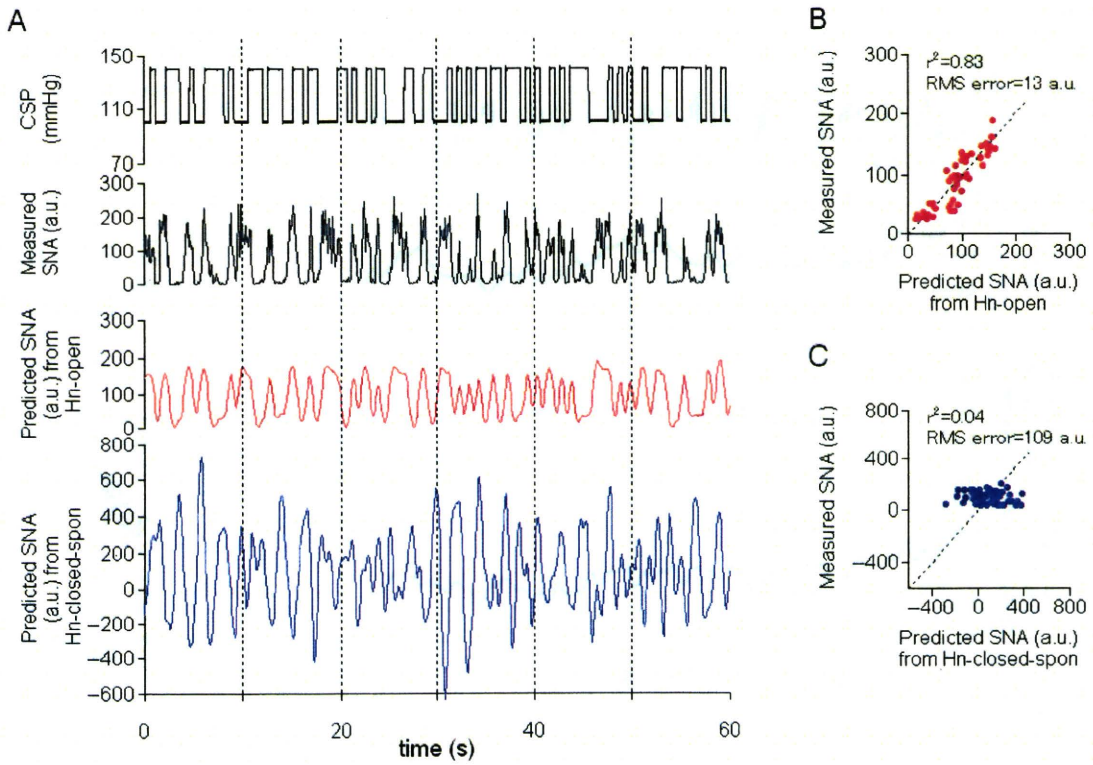

FIGURE 6

Figure 7

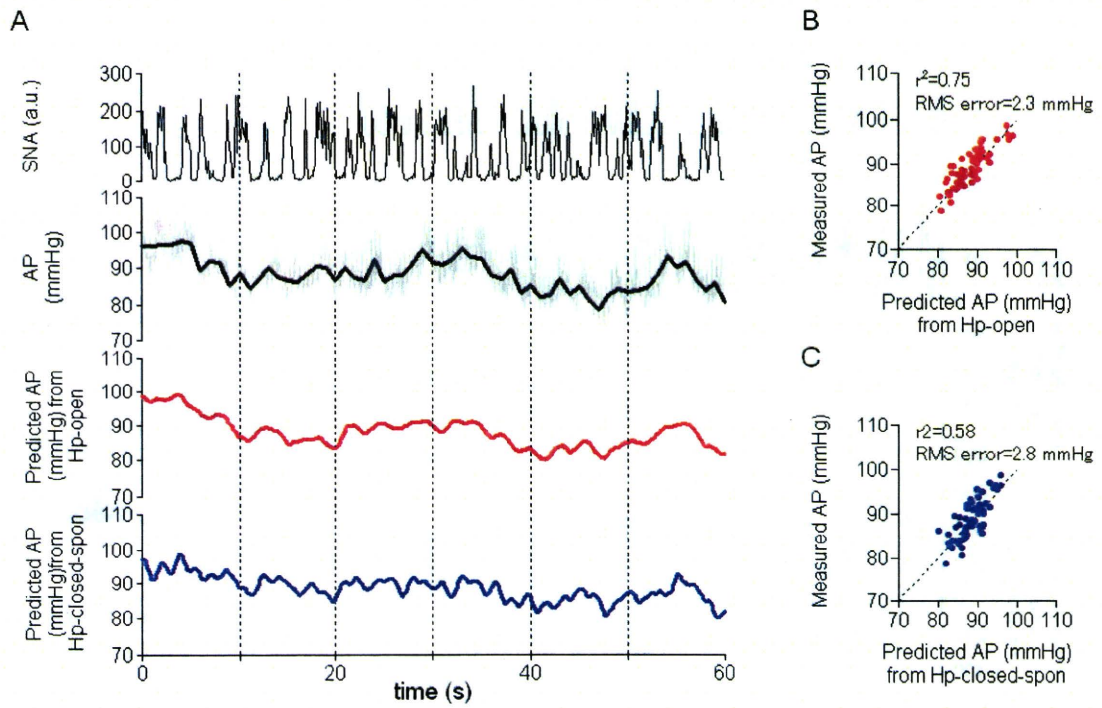

FIGURE 7

Figure 8

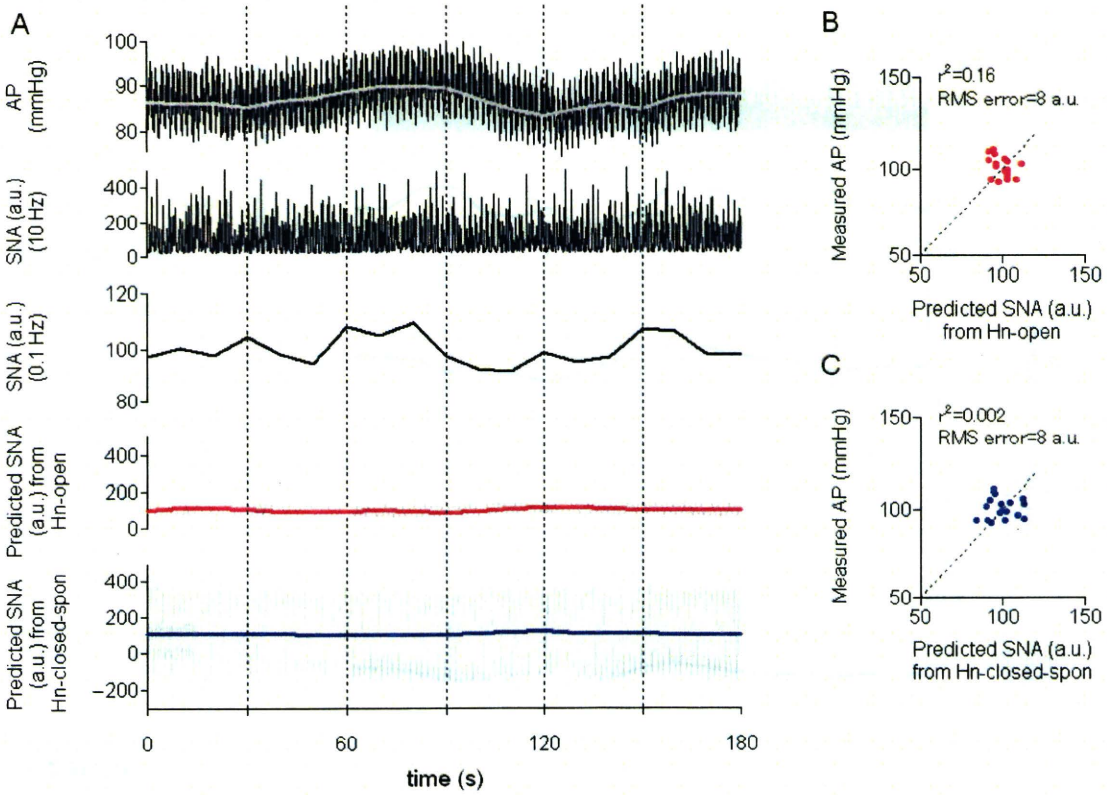

FIGURE 8

Figure 9

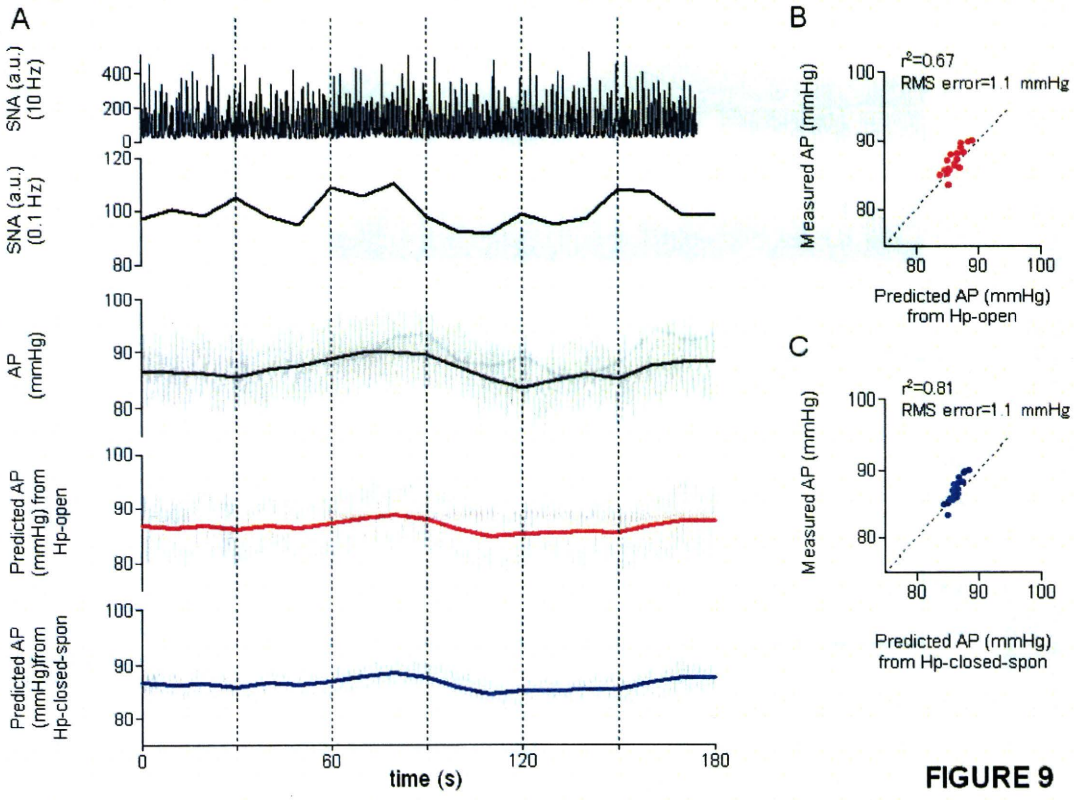

FIGURE 9

Figure 10

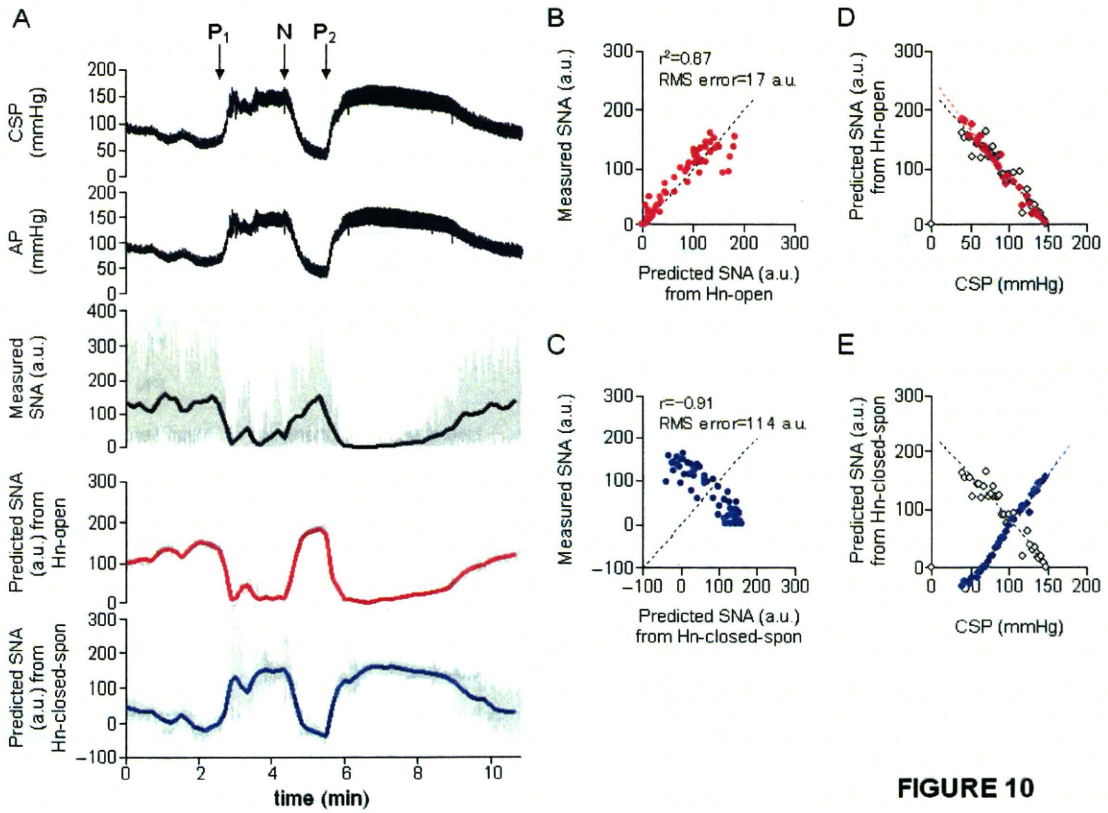

FIGURE 10

Figure 11

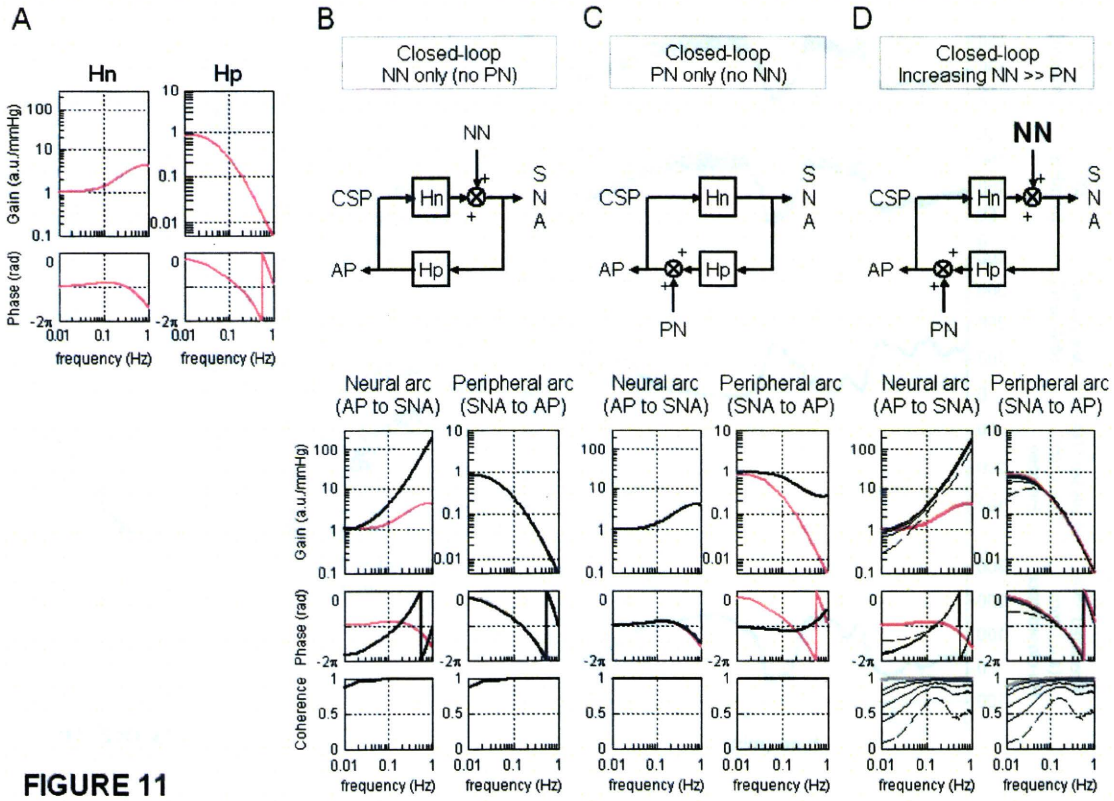

FIGURE 11

Articles in PresS. Am J Physiol Regul Integr Comp Physiol (January 26, 2011). doi:10.1152/ajpregu.00768.2010

Exercise training augments the dynamic heart rate response to vagal but not sympathetic stimulation in rats

Masaki Mizuno[1, 2], Toru Kawada[2], Atsunori Kamiya[2], Tadayoshi Miyamoto[2, 3], Shuji Shimizu[2], Toshiaki Shishido[2], Scott A. Smith[1], and Masaru Sugimachi[2]

[1]Departments of Physical Therapy and Internal Medicine, University of Texas Southwestern Medical Center at Dallas, Dallas, TX, USA; [2]Department of Cardiovascular Dynamics, National Cerebral and Cardiovascular Center Research Institute, Osaka, Japan; [3]Department of Physical Therapy, Morinomiya University of Medical Sciences, Osaka, Japan

Correspondence:
Masaki Mizuno, PhD
Department of Physical Therapy, University of Texas Southwestern Medical Center at Dallas, 5323 Harry Hines Blvd., Dallas, TX 75390-9174
Phone: 214-648-3294 Fax: 214-648-3566
Email: masaki.mizuno@utsouthwestern.edu

Running head: exercise training and dynamic autonomic heart rate control

Word count: 6,169
Figure: 5
Table: 6

Abstract

We examined the transfer function of autonomic heart rate (HR) control in anesthetized sedentary and exercise trained (16 weeks, treadmill for 1 h, 5 times/wk at 15m/min and 15° grade) rats for comparison to HR variability assessed in the conscious resting state. The transfer function from sympathetic stimulation to HR response was similar between groups (gain, 4.2 ± 1.5 vs. 4.5 ± 1.5 beats min^{-1} Hz^{-1}; natural frequency, 0.07 ± 0.01 vs. 0.08 ± 0.01 Hz; damping coefficient, 1.96 ± 0.55 vs. 1.69 ± 0.15; and lag time, 0.7 ± 0.1 vs. 0.6 ± 0.1 s, sedentary vs. exercise trained, respectively, mean ± SD). The transfer gain from vagal stimulation to HR response was 6.1 ± 3.0 in the sedentary and 9.7 ± 5.1 beats min^{-1} Hz^{-1} in the exercise trained group (P = 0.06). The corner frequency (0.11 ± 0.05 vs. 0.17 ± 0.09 Hz) and lag time (0.1 ± 0.1 vs. 0.2 ± 0.1 s) did not differ between groups. When the sympathetic transfer gain was averaged for very low frequency (VLF) and low frequency (LF) bands, no significant group effect was observed. In contrast, when the vagal transfer gain was averaged for VLF, LF, and high frequency bands, exercise training produced a significant group effect (P < 0.05 by two-way repeated measures ANOVA). These findings suggest that, in the frequency domain, exercise training augments the dynamic HR response to vagal stimulation but not sympathetic stimulation regardless of the frequency bands.

Keywords: exercise training; heart rate variability; transfer function; systems analysis; rats

Introduction

Heart rate variability (HRV) is considered to be a useful noninvasive assessment of autonomic nervous system activity. It has been well recognized that exercise training increases HRV at rest (4, 19). A recent meta-analysis by Sandercock et al. (28) demonstrated that exercise training results in significant increases in R-R interval and high frequency (HF) power of HRV. Nevertheless, not all studies have demonstrated increases in HRV after exercise training (7). To date, the exact mechanisms underlying increases in HRV after exercise training remain to be elucidated. Many earlier studies have suggested that the augmentation of HRV induced by exercise training may be caused by a withdrawal of sympathetic tonus and/or an increase in vagal tonus (5, 14, 36). Autonomic tone assessed by HRV may reflect both the autonomic outflow from the central nervous system and the peripheral autonomic regulation of atrial pacemaker cells. The latter can be assessed quantitatively by examining the heart rate (HR) response to electrical stimulation of the autonomic nerves. Further, recent studies suggested that peripheral autonomic regulation of atrial pacemaker cells could contribute to the exercise training-induced increases in cardiac vagal function (9, 10).

Equivocal results, however, have been reported using autonomic nerve stimulation. Regarding the vagal system, the effects of exercise training have been inconsistent among studies, showing both increases (9, 10) and reductions in vagally stimulated HR control (25). When considering the sympathetic system, a previous study demonstrated that the HR response to sympathetic stimulation was reduced by exercise training (22). However, the mechanisms underlying the training effect are controversial (3, 15, 26, 29, 33,